REPORT DOCUMENTATION PAGE

Form Approved
OMB No. 0704-0188

Public reporting burden for this collection of information is estimated to average 1 hour per response, including the time for reviewing instructions, searching existing data sources, gathering and maintaining the data needed, and completing and reviewing this collection of information. Send comments regarding this burden estimate or any other aspect of this collection of information, including suggestions for reducing this burden to Department of Defense, Washington Headquarters Services, Directorate for Information Operations and Reports (0704-0188), 1215 Jefferson Davis Highway, Suite 1204, Arlington, VA 22202-4302. Respondents should be aware that notwithstanding any other provision of law, no person shall be subject to any penalty for failing to comply with a collection of information if it does not display a currently valid OMB control number. **PLEASE DO NOT RETURN YOUR FORM TO THE ABOVE ADDRESS.**

1. REPORT DATE (DD-MM-YYYY)	2. REPORT TYPE Journal Article	3. DATES COVERED (From - To)

4. TITLE AND SUBTITLE	5a. CONTRACT NUMBER
A Two-Dimensional Fourth-Order CESE Method for the Euler Equations On Triangular Unstructured Meshes (Post-Print)	5b. GRANT NUMBER
	5c. PROGRAM ELEMENT NUMBER

6. AUTHOR(S)	5d. PROJECT NUMBER
David L. Bilyeu (AFRL); Yung-Yu Chen; S.-T. John Yu (Ohio State University)	5e. TASK NUMBER
	5f. WORK UNIT NUMBER Q02Z

7. PERFORMING ORGANIZATION NAME(S) AND ADDRESS(ES)	8. PERFORMING ORGANIZATION REPORT NO.
Air Force Research Laboratory (AFMC) AFRL/RQRS 1 Ara Drive Edwards AFB, CA 93524	

9. SPONSORING / MONITORING AGENCY NAME(S) AND ADDRESS(ES)	10. SPONSOR/MONITOR'S ACRONYM(S)
Air Force Research Laboratory (AFMC) AFRL/RQR 5 Pollux Drive Edwards AFB, CA 93524	11. SPONSOR/MONITOR'S REPORT NUMBER(S) **AFRL-RZ-ED-JA-2012-103**

12. DISTRIBUTION / AVAILABILITY STATEMENT
Approved for public release; distribution unlimited

14. ABSTRACT
Previously, Chang[1] reported a new high-order Conservation Element Solution Element (CESE) method for solving nonlinear, scalar, hyperbolic partial differential equations in one dimensional space. Bilyeu et al.[2] have extended Chang's scheme for solving a one-dimensional, coupled equations with an arbitrary order of accuracy. In the present paper, the one-dimensional, high-order CESE method is extended for two-dimensional unstructured meshes. A formulation is presented for solving the coupled equations with the fourth-order in accuracy. The new high-order CESE methods share many favorable attributes of the original second-order CESE method, including: (i) the use of compact mesh stencil involving only the immediate mesh nodes surrounding the node where the solution is sought,(ii) the CFL stability constraint remains to be ≤ 1, and (iii) superb shock capturing capability without using an approximate Riemann solver. To demonstrate the formulation, four test cases are reported, including (i) solution of a two-dimensional, scalar convection equation, (ii) the solution of the linear acoustic equations, (iii) the solution of the Euler equations for waves of small amplitudes, and (iv) the solution of the Euler equations for expanding shock waves. In all calculations, unstructured triangular meshes are used. In the first three cases, convergence tests show the fourth-order accuracy of the solutions. In the last case, numerical results of the fourth-order scheme are superior than that obtained by the second-order CESE method.

15. SUBJECT TERMS

16. SECURITY CLASSIFICATION OF:			17. LIMITATION OF ABSTRACT	18. NUMBER OF PAGES	19a. NAME OF RESPONSIBLE PERSON J-L Cambier
a. REPORT Unclassified	b. ABSTRACT Unclassified	c. THIS PAGE Unclassified	SAR	21	19b. TELEPHONE NO (include area code) 661 275-5649

Standard Form
298 (Rev. 8-98)
Prescribed by ANSI
Std. 239.18

50th AIAA Aerospace Sciences Meeting including the New Horizons Forum and Aerospace Exposition
09 - 12 January 2012, Nashville, Tennessee

AIAA 2012-0293

A Two-Dimensional Fourth-Order CESE Method for the Euler Equations on Triangular Unstructured Meshes

David L. Bilyeu,[*] Yung-Yu Chen, [†] and S.-T. John Yu [‡]

The Ohio State University, Columbus, OH 43210, USA

Previously, Chang[1] reported a new high-order Conservation Element Solution Element (CESE) method for solving nonlinear, scalar, hyperbolic partial differential equations in one dimensional space. Bilyeu et al.[2] have extended Chang's scheme for solving a one-dimensional, coupled equations with an arbitrary order of accuracy. In the present paper, the one-dimensional, high-order CESE method is extended for two-dimensional unstructured meshes. A formulation is presented for solving the coupled equations with the fourth-order in accuracy. The new high-order CESE methods share many favorable attributes of the original second-order CESE method, including: (i) the use of compact mesh stencil involving only the immediate mesh nodes surrounding the node where the solution is sought, (ii) the CFL stability constraint remains to be ≤ 1, and (iii) superb shock capturing capability without using an approximate Riemann solver. To demonstrate the formulation, four test cases are reported, including (i) solution of a two-dimensional, scalar convection equation, (ii) the solution of the linear acoustic equations, (iii) the solution of the Euler equations for waves of small amplitudes, and (iv) the solution of the Euler equations for expanding shock waves. In all calculations, unstructured triangular meshes are used. In the first three cases, convergence tests show the fourth-order accuracy of the solutions. In the last case, numerical results of the fourth-order scheme are superior than that obtained by the second-order CESE method.

I.   Introduction

In this paper, we extend the one-dimensional, high-order CESE method for solving two-dimensional coupled, nonlinear hyperbolic Partial Differential Equations (PDEs) by using unstructured meshes. The new formulation is currently fourth-order in accuracy, but it can be easily extended to a higher-order scheme by including more terms in the Taylor series expansion. The tenet of the CESE method is treating space and time in a unified manner in integrating the model equations for flux conservation. In the CESE method, the space-time domain is divided into non-overlapping Conservation Elements (CEs), over which the space-time integration is performed to enforce flux conservation. The integration is facilitated by using Solution Elements (SEs), which in general do not coincide with the CEs. The unknowns are discretized inside each SE by using a Taylor series expansion. Aided by the prescribed discretization schemes for the unknowns inside each SE, space-time flux over each surface of a CE can be calculated and the overall flux conservation over each CE can be enforced. The result is an explicit formulation for updating the unknowns for time-marching calculation. Special features of the CESE method include: (i) The unknowns are discretized by using the Taylor series expansion in both space and time. The order of the Taylor series is also the order of accuracy of the method. (ii) The method has the most compact mesh stencil, which involves only the immediate neighboring mesh points of the cell where the solution is sought. (iii) The method is an explicit scheme in time-marching calculation. The stability criterion is CFL ≤ 1. (iv) No approximate Riemann solver is used and the scheme is simple and efficient. (v) The CESE method includes a suite of numerical algorithms,

---

[*]Ph.D. Candidate, Dept. of Mechanical Engineering, bilyeu.4@osu.edu, and AIAA Student Member.
[†]Lead Developer of SOLVCON, yyc@solvcon.net.
[‡]Associate Professor, Dept. of Mechanical Engineering, yu.274@osu.edu and AIAA Member.

which are built based on the a scheme, a non-dissipative scheme. Extension of the a scheme involves various ways of adding artificial damping for maintaining numerical stability and for shock capturing.

The mesh stencil of the new, fourth-oder CESE method is identical to that in the second-oder CESE method.[4] For completeness, the treatment of unstructured triangular meshes is repeated here. Figure 1 is the projection of the space-time computational domain to the two-dimensional space. The solid lines represents the triangular mesh. Associated with each triangle, there are three CEs and the dashed lines are the boundaries of the CEs. The union of three CEs forms a composite CE, and point 3 is the centroid of the CE associated with cell j. Symbol squares represent the vertices of the mesh. The open circles are the centroids of triangles. The crosses are the centroids of the composite CEs. The solution is stored at the triangle centroid. Figures 2a and 2b show the CEs and SEs associated with the solution point $G(j)$, denoted by open a circle. These CEs are three-dimensional space-time regions, over which flux conservation is imposed. In each SE, the profiles of the unknowns are represented by a Taylor series expansion. For complete description of the geometry of CE and SE, please refer to.[4]

The remainder of the present paper is organized as follows. Section II present the numerical method for the time marching calculation. This section is broken up into four sub-sections: (i) calculation of the fluxes, (ii) calculation of the temporal derivatives, (iii) calculation of the even-order derivatives of the unknowns, and (iv) calculation of the odd-order derivatives of the unknowns. In Section III, we report numerical results obtained by using the new scheme. Finally, we present our concluding remarks and list the cited references.

II.   Numerical Method

The two-dimensional model equations to be solved are presented in the following vector-matrix form:

$$\frac{\partial \mathbf{U}}{\partial t} + \frac{\partial \mathbf{F}^x}{\partial x} + \frac{\partial \mathbf{F}^y}{\partial y} = 0 \tag{1}$$

where $\mathbf{U} = (u_1, u_2, \ldots, u_m)^t$, and $\mathbf{F}^{x,y} = (f_1^{x,y}, f_2^{x,y}, \ldots, f_m^{x,y})^t$, and there are m coupled equations in Eq. (1). Each equation in Eq. (1) can be recast into a divergence free condition: $\nabla \cdot \mathbf{h}_i = 0$, where $i = 1, \ldots, m$ and $\mathbf{h}_i = (f_i^x, f_i^y, u_i)^t$ is the space-time flux function of the ith equation. The divergence here operates in three-dimensional Euclidean space. Aided by the Gauss theorem, we have

$$\oint \mathbf{h}_i(x, y, t) \cdot d\mathbf{s} = 0. \tag{2}$$

The CESE method is a numerical method to integrate Eq. (2) while treating space and time in a unified manner. The integration is facilitated by the discretized conserved variables u_i and the fluxes $f_i^{x,y}$ with $i = 1, \ldots, m$. First, the space-time domain is divided into non-overlapping Conservation Element (CE). Over each CE, Eq. (2) is imposed. The actual integration is facilitated by the definition of Solution Elements (SE), in which u_i and $f_i^{x,y}$ are represented by Taylor series expansion. In deriving the formulation for integrating Eq. (2), we make the following assumptions: (i) Inside an SE, the unknowns and flux functions are discretized and they are represented by using a Taylor series. (ii) The desired order of convergences is even. In this paper, the fourth-order method will be developed. (iii) Each even-order derivative has an odd-order derivative with respect to each spatial direction. (iv) The discretized variables obey the alternative rule of differentiation, e.g., $\left(\partial^2 u_i / \partial x \partial y\right)^* = \left(\partial^2 u_i / \partial y \partial x\right)^*$, where the superscript $*$ denotes the discretized variables.

II.A.   The Taylor Series Expansion

To proceed, the conserved variables, $u_1, u_2, \ldots, u_m$, and the fluxes, $f_1^{x,y}, f_2^{x,y}, \ldots, f_m^{x,y}$ are discretized by using the Taylor series expansion in space and time. Shown below is the third-order Taylor expansion in

American Institute of Aeronautics and Astronautics

time and a two-dimensional space of a conserved variable u_i, where $1 \leq i \leq m$,

$$
\begin{aligned}
u_i(x, y, t) =& u_i(x_j, y_j, t^n) + (u_i)_x \Delta x + (u_i)_y \Delta y + (u_i)_t \Delta t + \\
& \frac{1}{2} \left[(u_i)_{xx} \Delta x^2 + 2(u_i)_{xy} \Delta x \Delta y + (u_i)_{yy} \Delta y^2 + 2(u_i)_{xt} \Delta x \Delta t + 2(u_i)_{yt} \Delta y \Delta t + (u_i)_{tt} \Delta t^2 \right] + \\
& \frac{1}{6} \left\{ (u_i)_{xxx} \Delta x^3 + (u_i)_{yyy} \Delta y^3 + \left[(u_i)_{xxy} + 2(u_i)_{xyx} \right] \Delta x^2 \Delta y + \left[2(u_i)_{xyy} + (u_i)_{yyx} \right] \Delta y^2 \Delta x + \right. \\
& 3(u_i)_{xxt} \Delta x^2 \Delta t + 3(u_i)_{xtt} \Delta x \Delta t^2 + 3(u_i)_{yyt} \Delta y^2 \Delta t + 3(u_i)_{ytt} \Delta y \Delta t^2 + \\
& \left. 6(u_i)_{xyt} \Delta x \Delta y \Delta t + (u_i)_{ttt} \Delta t^3 \right\}.
\end{aligned}
\tag{3}
$$

where the anchor point of the Taylor expansion is (x_j, y_j, t^n), and the distance is denoted by $\Delta x = x - x_j$, $\Delta y = y - y_j$, and $\Delta t = t - t^n$. Thus all derivatives are evaluated at (x_j, y_j, t^n). The above Taylor series can be written in a more concise form:

$$
u_i(x, y, t) = \sum_{a=0}^{N} \sum_{b=0}^{N-a} \sum_{c=0}^{N-a-b} \frac{\partial^{a+b+c} u_i}{\partial x^a \partial y^b \partial t^c} \frac{1}{a! b! c!} \Delta x^a \Delta y^b \Delta t^c,
\tag{4}
$$

where N is equal to the desired order of accuracy of the method minus 1. For the fourth-order CESE method, $N = 3$. Again, all derivatives on the right hand side of Eq. (4) are evaluated at (x_j, y_j, t^n). Moreover, in Eq. (4), we invoked assumptions (iii) and (iv), which lead to $\partial^2 u / \partial x \partial y = \partial^2 u / \partial y \partial x$ and $\partial^3 u / \partial x^2 \partial y \equiv (u_{xxy} + 2 u_{xyx})/3$, $\partial^3 u / \partial x \partial y^2 \equiv (2 u_{xyy} + u_{yyx})/3$ and so on. Similarly, the Taylor expansion of a derivative of the unknowns can be written as

$$
\frac{\partial^C u_i}{\partial x^I \partial y^J \partial t^K}(x, y, t) = \sum_{a=0}^{A} \sum_{b=0}^{A-a} \sum_{c=0}^{A-a-b} \frac{\partial^B u_i}{\partial x^{I+a} \partial y^{J+b} \partial t^{K+c}} \frac{1}{a! b! c!} \Delta x^a \Delta y^b \Delta t^c,
\tag{5}
$$

where $C = I + J + K$, $A = N - C$, and $B = C + a + b + c$. We remark that Eq. (4) is a special case of Eq. (5) with $A = N$. Similarly, the Taylor expansion of fluxes can be expressed as

$$
\frac{\partial^C f_i^{x,y}}{\partial x^I \partial y^J \partial t^K}(x, y, t) = \sum_{a=0}^{A} \sum_{b=0}^{A-a} \sum_{c=0}^{A-a-b} \frac{\partial^B f_i^{x,y}}{\partial x^{I+a} \partial y^{J+b} \partial t^{K+c}} \frac{1}{a! b! c!} \Delta x^a \Delta y^b \Delta t^c,
\tag{6}
$$

II.B. The Chain Rule

To proceed, we show the relationship between the derivatives of the fluxes $f_i^{x,y}$ and the derivatives of the conserved variables u_i, where $i = 1, \ldots, m$. Since $f_i^{x,y}$ are known functions of u_i, aided by the chain rule, the derivatives of $f_i^{x,y}$ can be related to the derivatives of u_i. For the first-order derivatives, we have

$$
\frac{\partial f_i^{x,y}}{\partial \Psi_1} = \sum_{l=1}^{m} \frac{\partial f_i^{x,y}}{\partial u_l} \frac{\partial u_l}{\partial \Psi_1},
\tag{7}
$$

where $\Psi_1 = x, y, t$. For the second-order derivatives, we have

$$
\frac{\partial^2 f_i^{x,y}}{\partial \Psi_1 \partial \Psi_2} = \sum_{l=1}^{m} \frac{\partial f_i^{x,y}}{\partial u_l} \frac{\partial^2 u_l}{\partial \Psi_1 \partial \Psi_2} + \sum_{l=1}^{m} \sum_{n=1}^{m} \frac{\partial^2 f_i^{x,y}}{\partial u_l \partial u_n} \frac{\partial u_l}{\partial \Psi_1} \frac{\partial u_n}{\partial \Psi_2}
\tag{8}
$$

where $(\Psi_1, \Psi_2) = (x, x), (y, y), (t, t), (x, y), (x, t)$, and (y, t). For the third-order derivatives, we have

$$
\begin{aligned}
\frac{\partial^3 f_i^{x,y}}{\partial \Psi_1 \partial \Psi_2 \partial \Psi_3} =& \sum_{l=1}^{m} \frac{\partial f_i^{x,y}}{\partial u_l} \frac{\partial^3 u_l}{\partial \Psi_1 \partial \Psi_2 \partial \Psi_3} + \\
& \sum_{l=1}^{m} \sum_{n=1}^{m} \frac{\partial^2 f_i^{x,y}}{\partial u_l \partial u_n} \left(\frac{\partial^2 u_l}{\partial \Psi_1 \partial \Psi_2} \frac{\partial u_n}{\partial \Psi_3} + \frac{\partial^2 u_l}{\partial \Psi_1 \partial \Psi_3} \frac{\partial u_n}{\partial \Psi_2} + \frac{\partial^2 u_l}{\partial \Psi_2 \partial \Psi_3} \frac{\partial u_n}{\partial \Psi_1} \right) + \\
& \sum_{l=1}^{m} \sum_{n=1}^{m} \sum_{p=1}^{m} \frac{\partial^3 f_i^{x,y}}{\partial u_l \partial u_n \partial u_p} \frac{\partial u_l}{\partial \Psi_1} \frac{\partial u_n}{\partial \Psi_2} \frac{\partial u_p}{\partial \Psi_3}
\end{aligned}
\tag{9}
$$

where $(\Psi_1, \Psi_2, \Psi_3) = (x, x, x), (y, y, y), (t, t, t), (x, y, t), (x, x, y), (y, y, t), (x, x, t), (x, y, y), (y, t, t)$, and (x, t, t). These equations are recursive and can be further extended for the high-order derivatives. Aided by Eqs. (7-9), the derivatives of $f_i^{x,y}$ are related to the derivatives of u_i.

American Institute of Aeronautics and Astronautics

II.C. Additional Equations

We proceed to obtain additional model equations by applying spatial and temporal differentiation to the original first-order governing equations Eq. (1):

$$
\begin{aligned}
\frac{\partial u_i}{\partial t} &= -\frac{\partial f_i^x}{\partial x} - \frac{\partial f_i^y}{\partial y}, \\
\frac{\partial}{\partial x}\left(\frac{\partial u_i}{\partial t}\right) &= -\frac{\partial^2 f_i^x}{\partial x \partial x} - \frac{\partial^2 f_i^y}{\partial y \partial x}, \\
\frac{\partial}{\partial y}\left(\frac{\partial u_i}{\partial t}\right) &= -\frac{\partial^2 f_i^x}{\partial x \partial y} - \frac{\partial^2 f_i^y}{\partial y \partial y}, \\
\frac{\partial}{\partial t}\left(\frac{\partial u_i}{\partial t}\right) &= -\frac{\partial^2 f_i^x}{\partial x \partial t} - \frac{\partial^2 f_i^y}{\partial y \partial t}.
\end{aligned}
\tag{10}
$$

Equation (10) can be extended to higher-order derivatives. In general, a derivative of u_i involving temporal differentiation can always be found by using the chain rule, i.e., Eqs. (7-9), in conjunction with the following generic formulation extended from Eq. (10):

$$
\frac{\partial^C u_i}{\partial x^I \partial y^J \partial t^K} = -\frac{\partial^C f_i^x}{\partial x^{I+1} \partial y^J \partial t^{K-1}} - \frac{\partial^C f_i^y}{\partial x^I \partial y^{J+1} \partial t^{K-1}},
\tag{11}
$$

where $C = I + J + K$, $K = 1, 2, \ldots, N$, $J = 0, 1, \ldots, N - K$, and $I = 0, 1, \ldots, N - K - J$. Equation (11) is a divergence-free condition the derivatives of space-time flux vector $\mathbf{h}_i$. Aided by the Gauss theorem, we have

$$
\oint \frac{\partial^{C-1}\mathbf{h}_i}{\partial x^I y^J t^{K-1}}(x, y, t) \cdot d\mathbf{s} = 0
\tag{12}
$$

Equation (2) is a special case of Eq. (12). To recapitulate, all derivatives of $f_i^{x,y}$ can be expressed by derivatives of u_i, and all temporal derivatives of u_i can be expressed in terms of the spatial derivatives of u_i. Therefore, as that in the original second-order CESE method, the independent variables in the high-order CESE method include only the conserved variables u_i and their spatial derivatives. Table 1 lists the primary unknowns of the fourth-order CESE method.

Table 1: Primary unknowns of a two-dimensional, fourth-order CESE method.

Even-order variables	Odd-order variables	
u_i	$(u_i)_x$	$(u_i)_y$
$(u_i)_{xx}$	$(u_i)_{xxx}$	$(u_i)_{xxy}$
$(u_i)_{xy}$	$(u_i)_{xyx}$	$(u_i)_{xyy}$
$(u_i)_{yy}$	$(u_i)_{yyx}$	$(u_i)_{yyy}$

II.D. Space-Time Flux Conservation

In this section, we integrate the original model equations, i.e., Eq. (2) as well as the additional equations Eq. (12) to find all even-order derivatives of the conserved variables. For the solution at the new time step by using the fourth-order CESE method, we integrate Eq. (2), i.e., the original equation, for u_i, and we integrate the following special cases of Eq. (12):

$$
\oint \frac{\partial^2 \mathbf{h}_i}{\partial x \partial x} \cdot d\mathbf{s} = 0, \quad \oint \frac{\partial^2 \mathbf{h}_i}{\partial x \partial y} \cdot d\mathbf{s} = 0, \quad \oint \frac{\partial^2 \mathbf{h}_i}{\partial y \partial y} \cdot d\mathbf{s} = 0
\tag{13}
$$

for the solutions of $(u_i)_{xx}$, $(u_i)_{xy}$, and $(u_i)_{yy}$, respectively. As will be shown in the following, the integration results in explicit formulation for the above unknowns. Once all the even-order unknowns of a given order are calculated, all the odd-order derivatives of the unknowns can be found by using a central-difference like procedure. Central differencing u_i results in the solution of $(u_i)_x$ and $(u_i)_y$, and central differencing $(u_i)_{xx}$ results in numerical solutions of $(u_i)_{xxx}$ and $(u_i)_{xxy}$, et cetera. This procedure is consistent with that in the

original second-order CESE method. The remainder of this subsection will focus on the calculation of flux conservation.

The even derivatives are found by conserving the flux through each CE. The calculation includes three steps: (i) the flux through the six side faces, (ii) the flux through the bottom face, and (iii) the flux through the top face. The flux through the side and bottom faces are calculated by using the known solutions at the previous time step at neighboring points of the current solution point. Therefore, the calculation for fluxes through side and bottom surfaces are explicit. The flux through the top surface is a function of the solution itself. In the following, the derivation is presented in two subsections for flux through side surface and through bottom/top surfaces.

II.D.1.   Flux Through Side Faces

Figure 3 shows the faces associated with the solution point $(x_{3\times}, y_{3\times})$. For a two-dimensional triangular mesh, there are three neighboring triangles surrounding the solution point $(x_{3\times}, y_{3\times})$. There are six side surfaces associated with the CE centered at $(x_{3\times}, y_{3\times})$. The centroids of three neighboring triangles are denoted by $(x_{1'}, y_{1'})$, $(x_{5'}, y_{5'})$, and $(x_{7'}, y_{7'})$. We note that points $1'$, $5'$, and $7'$ are not the solution points of the neighboring CEs. They are the centroids of the neighboring triangles. In the following, we denote the solution points associated with points $1'$, $5'$, and $7'$ by point $1'^{\times}$, $5'^{\times}$, and $7'^{\times}$. Extended from each of these centroids, a pair of side surfaces exist as a part of the surface of the CE centered at $(x_{3\times}, y_{3\times})$. On a side surface, the values of the conserved variables and fluxes can be calculated by the Taylor series expansion from the corresponding solution points, i.e., $(x_{1'^{\times}}, y_{1'^{\times}})$, $(x_{5'^{\times}}, y_{5'^{\times}})$, or $(x_{7'^{\times}}, y_{7'^{\times}})$.

To proceed, we consider point $(x_{1'}, y_{1'})$ and the two associated side surfaces spanned between $(x_{2'}, y_{2'})$ and $(x_{4'}, y_{4'})$. We will illustrate the calculation of one side surface spanned between $(x_{1'}, y_{1'})$ and $(x_{2'}, y_{2'})$ by using the Taylor series expansion from point $1'^{\times}$, which in general does not coincide with $(x_{1'}, y_{1'})$ unless all triangles all equilateral. We first calculate the coefficients of the Taylor series representing the fluxes. Then we integrate the Taylor series over the side surface to find the flux through the surface. At a location (x, y) on the side surface spanned by $(x_{1'}, y_{1'})$ and $(x_{2'}, y_{2'})$ and within $t^n - 1/2 \leq t \leq t^n$, the flux $f_i^{x,y}$ can be expressed as

$$(f_i^{x,y})^* = \sum_{a=0}^{A} \sum_{b=0}^{A-a} \sum_{c=0}^{A-a-b} \frac{\partial^{a+b+c} f_i^{x,y}}{\partial x^a \partial y^b \partial t^c} \frac{\Delta x^a \Delta y^b \Delta t^c}{a!b!c!}, \tag{14}$$

where $\Delta x = x - x_{1'^{\times}}$, $\Delta y = y - y_{1'^{\times}}$, and $\Delta t = t - t^{n-1/2}$. The superscript $*$ denotes the discretized variables. It understood that the derivatives of the flux function in the integrand are calculated at $(x_{1'^{\times}}, y_{1'^{\times}})$. Next we adopt the following notation to facilitate the integration:

$$\Delta x = \alpha(x_{2'} - x_{1'}) + x_{1'} - x_{1'^{\times}}, \quad \Delta y = \alpha(y_{2'} - y_{1'}) + y_{1'} - y_{1'^{\times}}, \quad \Delta t = \beta \frac{\Delta t}{2},$$

where $0 \leq \alpha \leq 1$, and $0 \leq \beta \leq 1$. A single spatial transformation variable is possible because the projection of the side face to the spatial domain is a straight line segment.

The unit normal vector on the side surface is $\mathbf{n} = [(y_{2'} - y_{1'}), -(x_{2'} - x_{1'}), 0]/\sqrt{(x_{2'} - x_{1'})^2 + (y_{2'} - y_{1'})^2}$. The differential area for the integration $dR = dsdt$, where $ds = d\alpha\sqrt{(x_{2'} - x_{1'})^2 + (y_{2'} - y_{1'})^2}$ and $dt = \Delta t/2 d\beta$ Aided by these definitions, the total flux through the side face can be expressed as

$$
\begin{aligned}
(F_i)_{1'2'21} &= \iint_{1'2'21}^{1} \mathbf{h}_i \cdot \mathbf{n} dR \\
&= \iint_{\alpha,\beta=0}^{1} [(f_i^x)^*, (f_i^y)^*, (u_i)^*] \cdot \left[(y_{2'} - y_{1'})\frac{\Delta t}{2}, -(x_{2'} - x_{1'})\frac{\Delta t}{2}, 0 \right] d\alpha d\beta \\
&= (y_{2'} - y_{1'})\frac{\Delta t}{2} \iint_{\alpha,\beta=0}^{1} (f_i^x)^* d\alpha d\beta - (x_{2'} - x_{1'})\frac{\Delta t}{2} \iint_{\alpha,\beta=0}^{1} (f_i^y)^* d\alpha d\beta.
\end{aligned}
\tag{15}
$$

The calculation in Eq. (15) depends on available solutions at point $1^{\times}$ at a previous time step. The calculation of fluxes through the other five side surface is similar to Eq. (15). As such, the flux through all side surfaces of the CE associated with the solution point $(x_{3\times}, y_{3\times})$ can be readily calculated:

$$(F_i)_{\text{side}} = (F_i)_{1'2'21} + (F_i)_{1'4'41} + (F_i)_{5'2'25} + (F_i)_{5'6'65} + (F_i)_{7'4'47} + (F_i)_{7'6'67}. \tag{16}$$

II.D.2.   Flux Through the Bottom Surface

To proceed, we present the calculation of the flux through the bottom surface of the CE centered at point $3^\times$. The bottom surface is at the old time step $n - 1/2$ and thus all points are denoted by the superscript $'$. The calculation of the flux through the bottom surface of the CE requires integration over three quadrilaterals. Again, we will only derive the calculation of the quadrilateral associated with points $1'$ and $1'^\times$ as shown in Fig. 4. In this figure, point $1'$ is the centroid of the neighboring triangle and point $3'$ is the centroid of central triangle. Points $2'$ and $4'$ are the shared vertices of triangles. To proceed, we split the quadrilateral into two triangles, i.e., $\Delta 1'3'4'$ and $\Delta 1'2'3'$.

To facilitate the integration, we first perform coordinate transformation that converts an arbitrary triangle into a right triangle. In the following discussions, we will only focus on triangle $\Delta 1'3'4'$ as shown in Fig. 4. The (x, y) coordinates are transformed to (ξ, η) with $(\xi_{1'}, \eta_{1'}) = (0, 0)$, $(\xi_{3'}, \eta_{3'}) = (1, 0)$, and $(\xi_{4'}, \eta_{4'}) = (0, 1)$. The transformation equation is

$$\begin{pmatrix} dx \\ dy \end{pmatrix} = \begin{pmatrix} x_\xi & x_\eta \\ y_\xi & y_\eta \end{pmatrix} \begin{pmatrix} d\xi \\ d\eta \end{pmatrix} \tag{17}$$

Assume all entries of the Jacobian matrix are constant and we have $x_\xi = (x_{3'} - x_{1'})/(1 - 0) = x_{3'} - x_{1'}$, $x_\eta = (x_{4'} - x_{1'})$, $y_\xi = (y_{3'} - y_{1'})$, and $y_\eta = (y_{4'} - y_{1'})$. By integrating Eq. (17) from point $1'^\times$, i.e., the solution point associated with the triangle centered at point 1 at $n - 1/2$ time step, to any other location (x, y) inside $\Delta 1'3'4'$, we have

$$\begin{pmatrix} x - x_{1'} \\ y - y_{1'} \end{pmatrix} = \begin{pmatrix} x_{3'} - x_{1'} & x_{4'} - x_{1'} \\ y_{3'} - y_{1'} & y_{4'} - y_{1'} \end{pmatrix} \begin{pmatrix} \xi \\ \eta \end{pmatrix} + \begin{pmatrix} x_{1'} - x_{1'^\times} \\ y_{1'} - y_{1'^\times} \end{pmatrix}$$

where $0 \leq \eta \leq 1$ and $0 \leq \xi \leq 1 - \eta$, and the Jacobian determinant of the coordinate transformation is

$$J = \left| \frac{\partial(x, y)}{\partial(\xi, \eta)} \right| = |(x_{3'} - x_{1'})(y_{4'} - y_{1'}) - (x_{4'} - x_{1'})(y_{3'} - y_{1'})|.$$

Aided by the coordinate transformation, the integration of the space-time flux $\mathbf{h}_i$ over triangle $\delta 1'3'4'$ can be expressed as

$$\begin{aligned}
(F_i)_{1'3'4'} &= \iint_{1'3'4'} \mathbf{h}_i \cdot \mathbf{n} dR \\
&= \iint_{\xi, \eta} [(f_i^x)^*, (f_i^y)^*, (u_i)^*] \cdot (0, 0, -1) J d\xi d\eta \\
&= -\iint_{\xi, \eta} (u_i)^* J d\xi \eta \\
&= -\int_0^1 \int_0^{1-\eta} \sum_{a=0}^A \sum_{b=0}^{A-a} \frac{1}{a!b!} \left(\frac{\partial^{a+b} u_m}{\partial x^a \partial y^b} \right)_{1'^\times} (\xi x_\xi + \eta x_\eta + \Delta x_1)^a (\xi y_\xi + \eta y_\eta + \Delta y_1)^b J d\xi d\eta.
\end{aligned} \tag{18}$$

where $\Delta x_1 = x_{1'} - x_{1^\times}$ and $\Delta y_1 = y_{1'} - y_{1^\times}$. Equation (18) can be readily calculated because all derivatives of u_i at point $1'^\times$, i.e., at the previous time step $t^{n-1/2}$, are known. The fluxes through triangle II as well as through other parallelepipeds associated with points $5'$ and $7'$ can be calculated in a similar manner. Thus the space-time flux through the whole bottom surface of the CE associated with point 3 can be readily calculated:

$$(F_i)_{\text{bot}} = (F_i)_{1'3'4'} + (F_i)_{1'2'3'} + (F_i)_{5'6'3'} + (F_i)_{5'3'2'} + (F_i)_{7'3'6'} + (F_i)_{7'4'3'}. \tag{19}$$

II.D.3.   Flux Through the Top Surface

The flux through the top surface of the CE associated with point 3 can be calculated in a like manner as that through the bottom surface of the CE. The difference is that the solution point, from which the Taylor series expansion is expanded, is point $3^\times$. Instead of using three solution points $1'$, $5'$, and $7'$ as that for the

flux through the bottom surface of the CE, only one solution point, i.e., point $3^\times$, is used for flux through the top surface:

$$
\begin{aligned}
(F_i)_{134} &= \iint_{134} \mathbf{h}_i \cdot \mathbf{n} dR \\
&= \iint_{\xi,\eta} [(f_i^x)^*, (f_i^y)^*, (u_i)^*] \cdot (0,0,1) J d\xi d\eta \\
&= \iint_{\xi,\eta} (u_i)^* J d\xi \eta \\
&= \int_0^1 \int_0^{1-\eta} \sum_{a=0}^{A} \sum_{b=0}^{A-a} \frac{1}{a!b!} \left(\frac{\partial^{a+b} u_m}{\partial x^a \partial y^b} \right)_{3\times} (\xi x_\xi + \eta x_\eta + \Delta x_3)^a (\xi y_\xi + \eta y_\eta + \Delta y_3)^b J d\xi d\eta.
\end{aligned}
\tag{20}
$$

where $\Delta x_3 = x_3 - x_{3\times}$ and $\Delta y_3 = y_3 - y_{3\times}$. Similar to that for the bottom surface, the total flux through the top surface is

$$
(F_i)_{\text{top}} = (F_i)_{134} + (F_i)_{123} + (F_i)_{563} + (F_i)_{532} + (F_i)_{736} + (F_i)_{743}.
\tag{21}
$$

Equation (21) is an implicit function of the conserved variable u_i and its spatial derivatives at point $3^\times$. For the fourth-order CESE method, the spatial derivatives of concerned are up to the third order. According to Table 1, there are total 12 even- and odd-order derivatives of u_i involved in Eqs. (20) and (21). In the following, we illustrate the procedure of integrating Eqs. (20) and (21) in several steps. In particular, we will show that all calculation steps involved are explicit; there is no need to solve the function implicitly, e.g., inverting a matrix.

First, we remark that point $3^\times$ is the centroid of the hexagonal area defined by points 125674, which is the top surface of the CE of concern. As such, the integration of the conserved variable $(u_i)_{3\times}$, i.e., the first term in the Taylor series expansion, over the entire top surface is simply $(u_i)_{3\times}$ multiplied by the hexagonal area, i.e., $(u_i)_{3\times} A_{\text{hex}}$, where A_{hex} denotes the area. Moreover, the integration of the first-order derivative terms in the Taylor series expansion, i.e., terms involving $(u_i)_x$, $(u_i)_y$, over A_{hex} would cancel out and be null. The same feature has been used in the development of the original second-order CESE method. Therefore, for the fourth-order CESE method, the space-time flux passing through the top surface of the CE, i.e., Eqs. (20) and (21), is an implicit function of $(u_i)_{3\times}$ and its second- and third-order derivatives. However, as will be shown in the following, these unknowns do not need to be solved simultaneously. Instead, we will solve for the second- and third-order derivatives of u_i first. Then, Eq. (21) becomes an explicit function of $(u_i)_{3\times}$ only.

To proceed, we integrate three additional model equations shown in Eq. (13) to calculate $(u_i)_{xx}, (u_i)_{xy}$, and $(u_i)_{yy}$ and their first-order derivatives, i.e., the third-order derivatives of u_i, at point $3^\times$. To this end, we simply apply the original second-order CESE method three times for space-time flux conservation of $(u_i)_{xx}, (u_i)_{xy}$, and $(u_i)_{yy}$. Although flux conservation of these three variables are not prescribed by the original model equations, the invoked assumption of smoothness and differentiable of the primary unknowns u_i up to the third-order would ensure the validity of these three additional conservation equations. The procedure of solving the second- and third-order derivatives of u_i is identical to that of the original, second-order CESE method for solving u_i and its first-order derivatives. For conciseness, no discussion about the integration procedure is repeated here.

With the known second- and third-order derivatives of $(u_i)_{3\times}$, Eq. (21) becomes an explicit function of the conserved variable of $(u_i)_{3\times}$ at the solution point,

$$
(u_i)_{3\times} = \frac{-1}{A_{\text{hex}}} \left[(F_i)_{\text{side}} + (F_i)_{\text{bot}} + (F_i)_{\text{top,2nd,3rd}} \right]
\tag{22}
$$

where $(F_i)_{\text{top,2nd,3rd}}$ denotes the part of the space-time flux in Eq. (21), which can be calculated by using the known second- and third-order derivatives of u_i.

The integrals in Eqs. (15), (18), and (20) can be explicitly calculated in several different manners. In this work, we calculate the integrals by using a symbolic mathematic package. As such all unknowns in the fourth-order CESE method are calculated except the first-order derivative of u_i. The algorithm of calculating the first-order derivatives is identical to that of the second-order CESE method. Essentially,

American Institute of Aeronautics and Astronautics

based on the known even-order derivatives (one order lower than the desired odd-order derivatives), a central-differencing procedure is applied to the even-order derivatives to calculate the odd-order derivatives. The same algorithm is used to calculate third-order derivatives based on the known second-order derivatives in the above fourth-order CESE method. For completeness, the central difference method is illustrated in the following subsection.

II.D.4. Odd-Order Derivatives

The odd-order derivatives of the conserved variables are calculated by using a central-differencing method, which is identical to that used in the original, second-order CESE method.[4–6] The mesh stencil employed for calculating the odd derivatives is shown in Fig. 5, in which symbol squares denote vertices of triangles, crosses denote solution points, and plus signs the shifted locations of the solutions points for the CFL insensitive schemes. The spatial location of shifted solution points (the plus sign) are calculated by

$$(x_{j+}, y_{j+}) = \left[\tau(x_{3\times} - x_{j\times}) + x_{j\times}, \tau(y_{3\times} - y_{j\times}) + y_{j\times}\right], \tag{23}$$

where $j = 1, 5, 7$ indicate the three neighbors of the CE centered at point $3^\times$ where the solution at a new time step is sought, τ is a function of the local CFL number, $(x_{j\times}, y_{j\times})$, with $j = 1, 5, 7$, are the original solution points of the three neighbors, and (x_{j+}, y_{j+}), with $j = 1, 5, 7$, are the shifted solution points of the three neighbors. The solutions at the previous time step $n - 1/2$ to be used for the time marching calculation are stored at $(x_{j\times}, y_{j\times})$, with $j = 1, 5, 7$. Thus, we first take a Taylor expansion from $(x_{j\times}, y_{j\times})$ at the time level $n - 1/2$ to the shifted locations (x_{j+}, y_{j+}) at the new time level n:

$$\left[(u_i)_{x^I y^J}\right]_{j+}^n \approx \sum_{a=0}^{A} \sum_{b=0}^{A-a} \sum_{c=0}^{A-a-b} \left(\frac{\partial^B u_i}{\partial x^{I+a} \partial y^{J+b} \partial t^{k+c}}\right)_{j\times}^{n-\frac{1}{2}} \frac{1}{a!b!c!} \left(x_{j+} - x_{j\times}\right)^a \left(y_{j+} - y_{j\times}\right)^b \left(\frac{\Delta t}{2}\right)^c. \tag{24}$$

Aided by Eq. (24) solutions of unknowns at the three shifted solution points in the new time level are calculated. The four points 1^+, 5^+, 7^+, and $3^\times$ form three triangles. Consider triangle $\Delta 3^\times 1^+ 5^+$. The spatial derivatives of the unknowns in this triangle can be readily calculated:

$$\begin{bmatrix} x_{1+} - x_{3\times} & y_{1+} - y_{3\times} \\ x_{5+} - x_{3\times} & y_{5+} - y_{3\times} \end{bmatrix} \begin{bmatrix} (u_i)_{x^{I+1} y^J} \\ (u_i)_{x^I y^{J+1}} \end{bmatrix} = \begin{bmatrix} \left[(u_i)_{x^I y^J}\right]_{1+}^n - \left[(u_i)_{x^I y^J}\right]_{3\times}^n \\ \left[(u_i)_{x^I y^J}\right]_{5+}^n - \left[(u_i)_{x^I y^J}\right]_{3\times}^n \end{bmatrix} \tag{25}$$

Similar calculation as that in Eqs. (25) and (24) can be performed to find the odd-order derivatives $[(u_i)_{x^{I+1} y^J}$, $(u_i)_{x^I y^{J+1}}]$ in triangles $\Delta 3^\times 7^+ 5^+$ and $\Delta 3^\times 1^+ 7^+$. For shock capturing, these three sets of odd-order derivatives are weighted by using the following formula:

$$(u_i)_{x^{I+1} y^J} = W \left\{ \left[(u_i)_{x^{I+1} y^J}\right]^{(1)}, \left[(u_i)_{x^{I+1} y^J}\right]^{(2)}, \left[(u_i)_{x^{I+1} y^J}\right]^{(3)}, \alpha \right\} \tag{26}$$

$$(u_i)_{x^I y^{J+1}} = W \left\{ \left[(u_i)_{x^I y^{J+1}}\right]^{(1)}, \left[(u_i)_{x^I y^{J+1}}\right]^{(2)}, \left[(u_i)_{x^I y^{J+1}}\right]^{(3)}, \alpha \right\} \tag{27}$$

where the superscript (r) with $r = 1, 2, 3$ denotes the three triangles $\Delta 3^\times 1^+ 5^+$, $\Delta 3^\times 7^+ 5^+$a, and $\Delta 3^\times 1^+ 7^+$, and the weighting function W is defined as

$$W = (\mu, \sigma, \psi, \alpha) = \frac{(\theta_2 \theta_3)^\alpha \mu + (\theta_3 \theta_1)^\alpha \sigma + (\theta_1 \theta_2)^\alpha \psi}{(\theta_1 \theta_2)^\alpha + (\theta_2 \theta_3)^\alpha + (\theta_3 \theta_1)^\alpha}, \tag{28}$$

where θ is the magnitude of the odd-order derivative vector:

$$\theta_r = \sqrt{\left\{\left[(u_i)_{x^{I+1} y^J}\right]^{(r)}\right\}^2 + \left\{\left[(u_i)_{x^I y^{J+1}}\right]^{(r)}\right\}^2}. \tag{29}$$

Equations (24-**??**) are used to calculate the odd-order derivatives of the conserved variables to the new time step. Shown in the above equations, the calculation of the odd-order derivatives depend on the even-order derivatives of the next lower order. To recapitulate, the algorithm of the fourth-order CESE method can be organized in the following steps: (i) Apply the original second-order CESE method three times to solve for the additional equations in terms of the second-order derivatives of u_i as shown in Eq. (13) for

the solution of the second-order derivatives based on the space-time flux conservation. (ii) Calculate all the third-order derivatives by central differencing the solutions of the second-order derivatives. (iii) Apply the newly developed fourth-oder CESE method to calculate the zero-order derivatives, or the conserved variables themselves. (iv) Finally, we calculate the first-order derivatives by central differencing the conserved variables.

The above recursive algorithm can be extended to sixth- or even higher-order methods. The mesh stencils employed for all high-order methods is identical to that used for the original CESE method. For the sixth-order CESE method, we first repeatedly apply the second-order CESE method to solve for all the fourth-order derivatives of u_i. Then, the fourth-orders derivatives are central differenced to obtain the fifth-order derivatives. Next, we would apply the fourth-order method three times to solve for all the second-order derivatives, followed by central difference procedure for the third-order derivatives. Finally, one can apply the six-order CESE method to calculate the conserved variables, followed by central difference procedure for the second-order derivatives.

III.   Results and Discussion

In this section, we report the numerical results obtained by applying the newly developed, two-dimensional, fourth-order CESE method. Three sets of model equations are considered, including (i) a scalar convection equation, (ii) the linearized Euler equations for acoustics, and (iii) the Euler equations. Numerical results of four cases are reported: one case each for solving the scalar equation and the acoustic equations, and two cases for solving the Euler equations. In all four cases, the third-order Taylor series is used to discretize the conserved unknowns and the fluxes inside each SE. Thus, the numerical scheme employed is fourth-order in accuracy. To determine the convergence rates, we measure the L_2 norm of errors. For a conserved variable u_i, the nth norm L_n with $n = 1$ or 2, is defined as

$$L_n = \sqrt[n]{\sum_j \left[(u_i)_{j,\text{num}} - (u_i)_{j,\text{ana}} \right]^n A_j},$$

where the subscript num denotes the numerical result, ana the analytical solution, and A_j is the area of cell j. The order of accuracy of the numerical results is assessed by the convergence test. We repeat the same simulation with several sets of meshes with decreasing cell sizes. The convergence tests are performed for the first three cases, which involve linear solutions. In the fourth case, the solution involves shock waves. In the vicinity of shocks, a reweighing function is activated and artificial damping is added to solutions so that oscillations of solution in the near shock region would be suppressed. Thus the order of accuracy would be reduced to be first-order around the shock wave.

Each convergence test is done by using two types of meshes: (i) uniform meshes that is created by splitting a quad mesh into 4 triangles, (ii) unstructured meshes composed of random triangles. We used Cubit[a] a DoE package developed by using the advancing-front algorithm, to generate all meshes. For the uniform meshes the option of QTri mesh, provided by Cubic was used. For the unstructured meshes the option of TriAdvance was used. In using the TriAdvance algorithm, we first employed the Delaunay algorithm to generate the preliminary meshes. We then use the QTri method to refine the meshes. The remainder of this section reports the numerical results of the four cases.

III.A.   The Scalar Advection Equation

The equation of concern is

$$\frac{\partial u}{\partial t} + a_x \frac{\partial u}{\partial x} + a_y \frac{\partial u}{\partial y} = 0.$$

A square domain $-\pi \leq x \leq \pi$, $-\pi \leq y \leq \pi$ is considered. Periodic boundary conditions are imposed to all four sides of the computational domain. The initial condition is $u(x, y, 0) = \sin(a_x x + a_y y)$. Due to the periodic condition, the analytical solution $u_{\text{ana}} = \sin(a_x x + a_y y + a_t t)$, with $a_t = -\sqrt{a_x^2 + a_y^2}$. In the present calculation, we let $a_x = a_y = 1$. In calculation, we let the simulation run until $t = 15$, and the CFL

---

[a]http://cubit.sandia.gov/index.html

American Institute of Aeronautics and Astronautics

number ≈ 1. Table 2 shows the calculated convergence rate by using the newly developed fourth-order CESE method. Table 2(a) shows the results of using uniform meshes and the convergence up to fifth order is found. Table 2(b) shows results of using unstructured triangular meshes and the convergence rate is fourth-order. When calculating the convergence rates for the uniform meshes, the characteristic length employed is the square root of the area of each triangular cell. For unstructured meshes, it is the square root of the area of the largest triangular cell in the mesh.

Table 2: Convergence rates of the fourth-order CESE method for solving the scalar advection equation.

(a) Structured grid

number of cells	h	L_2 error	$O(L_2)$
400	9.870E-02	2.158E-01	-
1600	2.467E-02	6.726E-03	5.00
3600	1.097E-02	8.762E-04	5.03
6400	6.169E-03	2.065E-04	5.02
10000	3.948E-03	6.735E-05	5.02

(b) Unstructured grid

number of cells	h	L_2 error	$O(L_2)$
232	1.690E-01	2.929E-01	-
926	4.255E-02	9.727E-03	4.94
2068	1.909E-02	1.315E-03	4.99
3694	1.068E-02	3.131E-04	4.94
5774	6.835E-03	1.022E-04	5.01

III.B.   The Linear Acoustic Equations

The acoustic equations are the linearized Euler equations for compressible flows:

$$\frac{\partial \rho}{\partial t} + \rho_0 \left(\frac{\partial v_x}{\partial x} + \frac{\partial v_x}{\partial x} \right) = 0$$

$$\frac{\partial v_x}{\partial t} + \frac{a_0^2}{\rho_0} \frac{\partial \rho}{\partial x} = 0$$

$$\frac{\partial v_y}{\partial t} + \frac{a_0^2}{\rho_0} \frac{\partial \rho}{\partial y} = 0,$$

where ρ, v_x, v_y, a_0, and ρ_0 are respectively the density, x and y component of the velocity, the speed of sound of the free stream, and the density of the free stream. A square domain is considered: $-2\pi \leq x \leq 2\pi$ and $-2\pi \leq y \leq 2\pi$. We then impose the periodic boundary conditions to the four sides of the computational domain. When $t = 0$, the initial conditions are

$$\rho(x, y, 0) = \rho_0 + \rho' \sin(a_x x + a_y y)$$

$$v_x(x, y, 0) = -a_0^2 \frac{\rho'}{\rho_0} \frac{a_x}{a_t} \sin(a_x x + a_y y)$$

$$v_y(x, y, 0) = -a_0^2 \frac{\rho'}{\rho_0} \frac{a_y}{a_t} \sin(a_x x + a_y y),$$

where ρ' is a prescribed amplitude of the perturbation. As such, the analytical solution is

$$\rho_{\text{ana}} = \rho_0 + \rho' \sin(a_x x + a_y y + a_t t)$$

$$(v_x)_{\text{ana}} = -a_0^2 \frac{\rho'}{\rho_0} \frac{a_x}{a_t} \sin(a_x x + a_y y + a_t t)$$

$$(v_y)_{\text{ana}} = -a_0^2 \frac{\rho'}{\rho_0} \frac{a_y}{a_t} \sin(a_x x + a_y y + a_t t),$$

American Institute of Aeronautics and Astronautics

where $a_t = -a_0\sqrt{a_x^2 + a_y^2}$. In this test case, we let $a_x = a_y = 1$, $\rho' = 0.01$, $a_0 = \rho_0 = 1.0$. The time-marching calculation is run until $t = 18$. The CFL number is about 0.7 for the case using the unstructured mesh, and about 0.75 for the case using the uniform mesh.

Shown in Fig. 6, the convergence rate is approximately 4.3 for the unstructured-mesh case, and 4.6 for the uniform-mesh case. The convergence rate for the non-uniform case includes the four most courses simulations. In the figure, h denote the length scale of a typical mesh cell, i.e., $h \approx \Delta x \approx \Delta y$. For similar h, the result obtained by using the unstructured mesh tends to be more accurate than that by using the structured mesh. This is true up until an h value of 0.1. At this point the L_2 norm for the unstructured mesh begins to increase. The sudden decrease in the convergence rate was further investigated by the Euler equation.

III.C.   The Euler Equations for Linear Waves

This section reports numerical results of the two-dimensional Euler equations obtained by using the fourth-order CESE method. Two cases are included. The first one is related to linear waves, which are used to determine the convergence rate of the solver. The second test shows the shock capturing capabilities of the new solver. For the linear wave case, the following initial conditions are used:

$$\rho(x,y,0) = 1.0 + 0.002\sin(a_x x + a_y y + a_t t)$$
$$v_x(x,y,0) = 0.5 \quad v_y(x,y,0) = 0.5 \quad p(x,y,0) = 2^{4/3}/\gamma$$

where $a_x = a_y = \pi$ and $a_t = -(a_x V_x + a_y V_y)$. The computational domain is $2 \le x \le 2, -2 \le y \le 2$. The calculation is done for time period of $0 \le t \le 4$. The total time period of 4 corresponds to 2 periods of wave. The periodic boundary condition is imposed to the four sides of the square domain.

For the convergence test, the numerical solution of the fourth-order CESE method was compared with that of the second-order CESE method. Shown in Fig. 7, the second-order simulation achieves a convergence rate of 3.1, while the fourth-order simulations achieves a convergence rate of 4.1. When the L_1 norm is used, the convergence rates decrease by one for both cases. When the L_∞ norm is used, the convergence rate increases by one. For all convergence rates, the characteristic size h is equal to the square root of the averaged areas of all cells. In all cases, the CFL number varies between 0.5 and 0.8.

III.D.   The Euler Equations for an Expanding Shock

In this case, the new fourth-order CESE method has been used to simulate a compressible flow with shock wave. The computational domain is a square. The length of each side is 2. Non-reflecting boundary condition is imposed to all four sides of the computational domain. The initial conditions is a two-dimensional set up of a shock tube. Inside the radius $r \le R_0$, pressure and density are higher than that outside of the radius, i.e., $r \ge R_0$.

$$\rho, p = \begin{cases} 1.0, 1.0 \text{ if } r < R_0 \\ 0.125, 0.1 \text{ if } r \ge R_0 \end{cases};$$

where $r = \sqrt{(x - x_0)^2 + (y - y_0)^2}$, $R_0 = 0.5$, and (x_0, y_0) is the center of the high-pressure domain. At the beginning of the simulation, the diaphragm separating the high pressure region and the low pressure region is lifted and a shock wave expands outwards and a expansion wave converges towards the center. This case was simulated by using both the second- and fourth-order CESE solvers. When running the fourth-order simulations it was found that the current suite of limiters commonly used in the second-order CESE method were not potent enough to maintain stability.

A new limiter was developed that insures that the Taylor series convergences. This is accomplished by looking at the influence that the next higher derivatives has on the summation of the lower derivatives in

the Taylor series.

$$\left| \left(\frac{\partial u^{I+J+1}}{\partial x^{I+1} \partial y^J} \right)^* \right| h \leq \beta \left| \sum_{i=0}^{I} \sum_{j=0}^{J-i} \left(\frac{\partial u^{i+j}}{\partial x^i \partial y^j} \right)^* \right| \frac{h^{i+j}}{i!j!} \text{ and}$$

$$\left| \left(\frac{\partial u^{I+J+1}}{\partial x^I \partial y^{J+1}} \right)^* \right| h \leq \beta \left| \sum_{i=0}^{I} \sum_{j=0}^{J-i} \left(\frac{\partial u^{i+j}}{\partial x^i \partial y^j} \right)^* \right| \frac{h^{i+j}}{i!j!}$$

where h is the square root of the cell area, β is an adjustable parameter on the order of 1. If this check does not pass, the higher-order derivative is set to be null. This check is done twice. First after the second and third derivatives are calculated, then again after the zero and first derivatives are calculated. It should be noted that this test is done in addition to the weighted odd derivative calculation expressed in Eq. 28.

This case of shock wave was tested by using three different meshes with 5770, 23000 and 91754 cells. The results can be seen in Fig. 10. The results from the fourth-order CESE scheme were compared to the second-order CESE scheme. The plots shown in Fig. 10 are the values plotted along a line going from the lower left to the upper right corners. In all cases the fourth-order solution has more dissipation near the middle of the domain. For the 5770 cell case the second-order version was not able to produce the correct shock and contact location, while the fourth-order version was able to. For the other two cases the results are very similar with, the fourth-order version has slightly sharper contacts but more dissipation towards the center of the domain. This dissipation decreases as the resolution increases. In all cases the value of β was 1 and α was 2. The average CFL number were 0.84, 0.88 and 0.93 for the 5770, 23000 and 91754 cases respectively.

IV. Concluding Remarks

This paper reports a new fourth-order CESE method for solving the two-dimensional linear and nonlinear hyperbolic partial differential equations by using unstructured meshes. The method is an extension of Chang's high-order CESE methods for one-dimensional equations. The method here focuses on the use of unstructured triangular meshes for solving a set of coupled equations. The new fourth-order CESE method retains all favorable features of the original second-order CESE method, including (i) the use of the most compact mesh stencil involving only the immediate neighboring nodes of the central node where the unknowns are sought, (ii) the stability constraint of the four-order CESE method remains to be CFL $\leq$ 1, and (iii) completely explicit operation in the time marching calculation. Moreover, the presented formulation is general and recursive; it can be easily extended to the sixth- or a even higher-oder CESE method. To demonstrate the capabilities of the new method, we have reported numerical solutions of three different sets of model equations, including the scalar advection equation, the acoustic equations, and the Euler equations. For solutions of linear problems, we demonstrated fourth-order convergence rates by using completely unstructured meshes. When using a uniform mesh, numerical results show super convergence. We have also solved the Euler equations for modeling supersonic flows with shocks. Numerical results of an expanding shock demonstrated that, by using the original reweighing function as that in the original second-order CESE method to the first- and third-order derivatives, the new fourth-order CESE method can accurately capture moving shock waves.

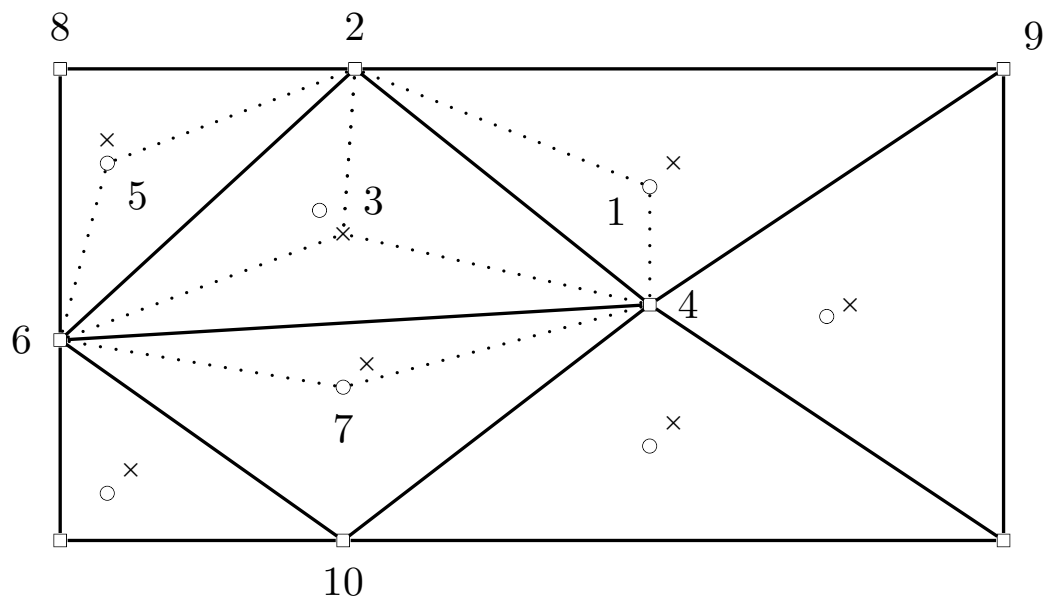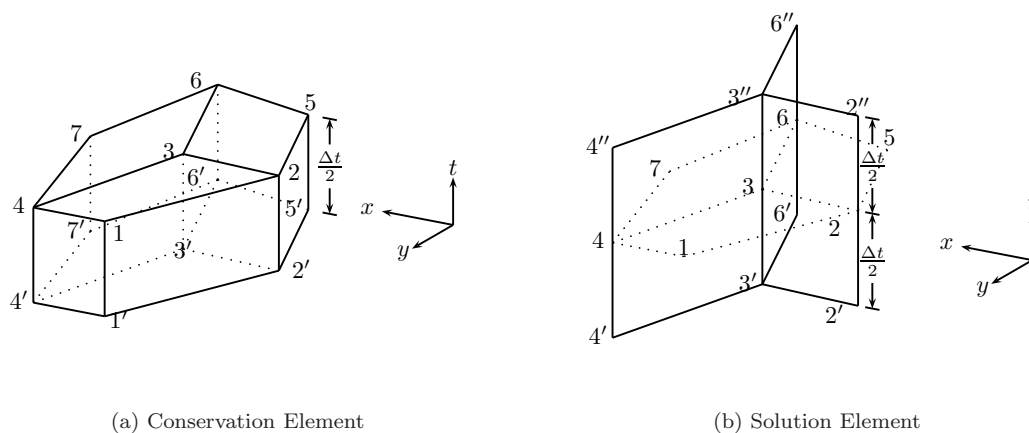American Institute of Aeronautics and Astronautics

Fig. 1: The CESE domain using a triangular mesh with points of interest marked by squares(cell vertices), circles(cell centroid) and crosses(CE centroid/solution point).

(a) Conservation Element

(b) Solution Element

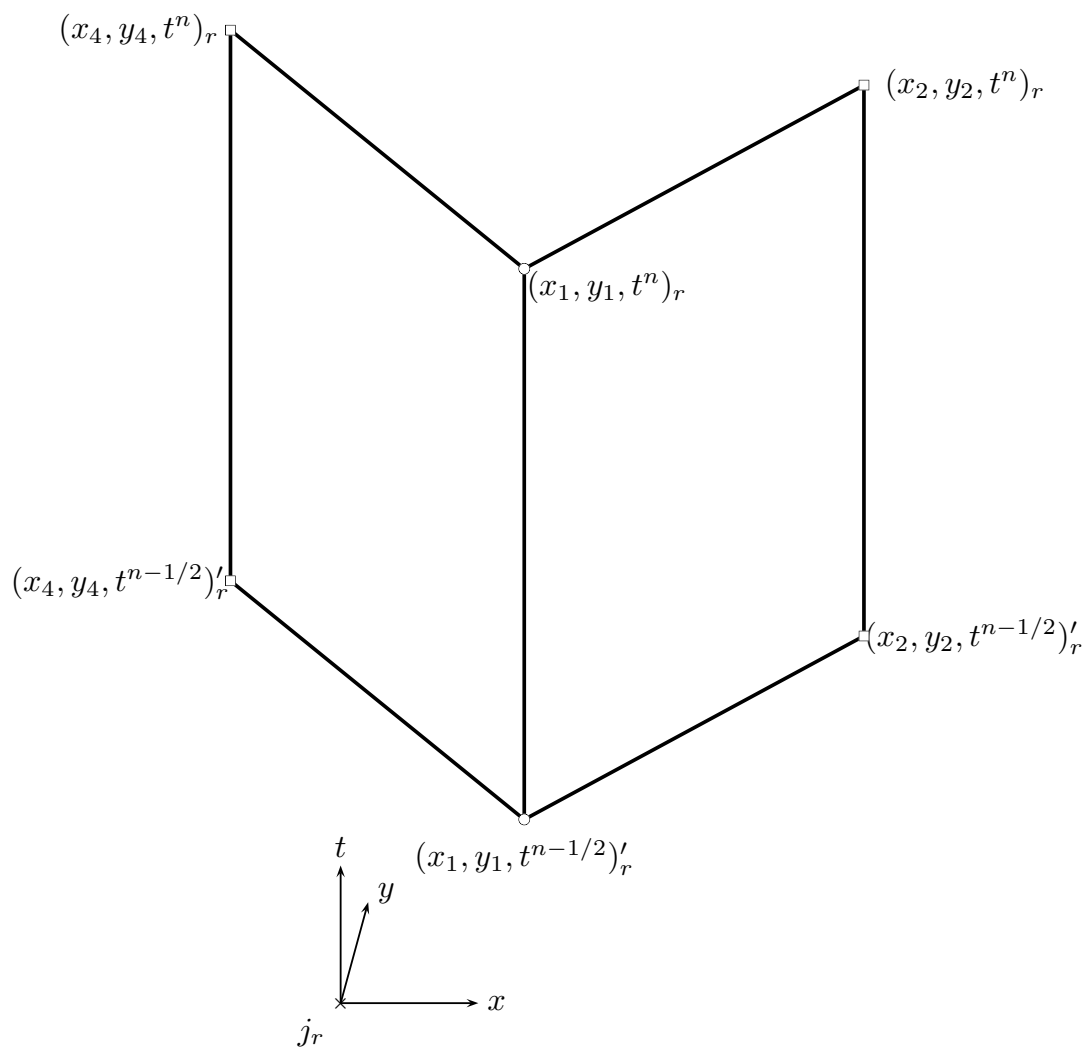Fig. 2: The CE and SE centered on the centroid mesh point (j,n).

American Institute of Aeronautics and Astronautics

V. Figures

Fig. 3: The side faces associated with a solution point
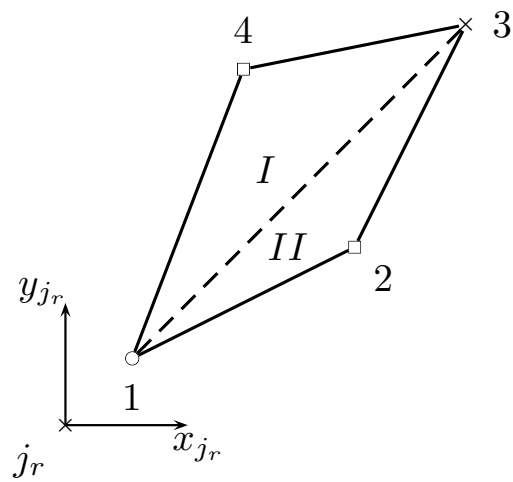
Fig. 4: The bottom face and top face
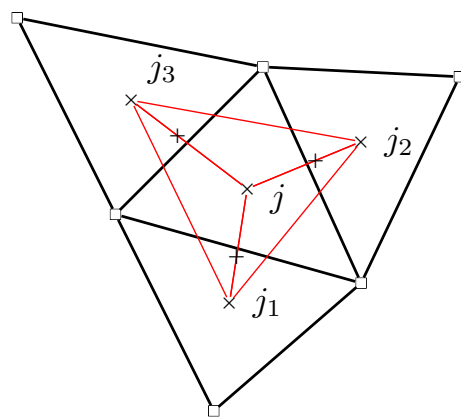
Fig. 5: The stencils used for the odd derivatives

American Institute of Aeronautics and Astronautics
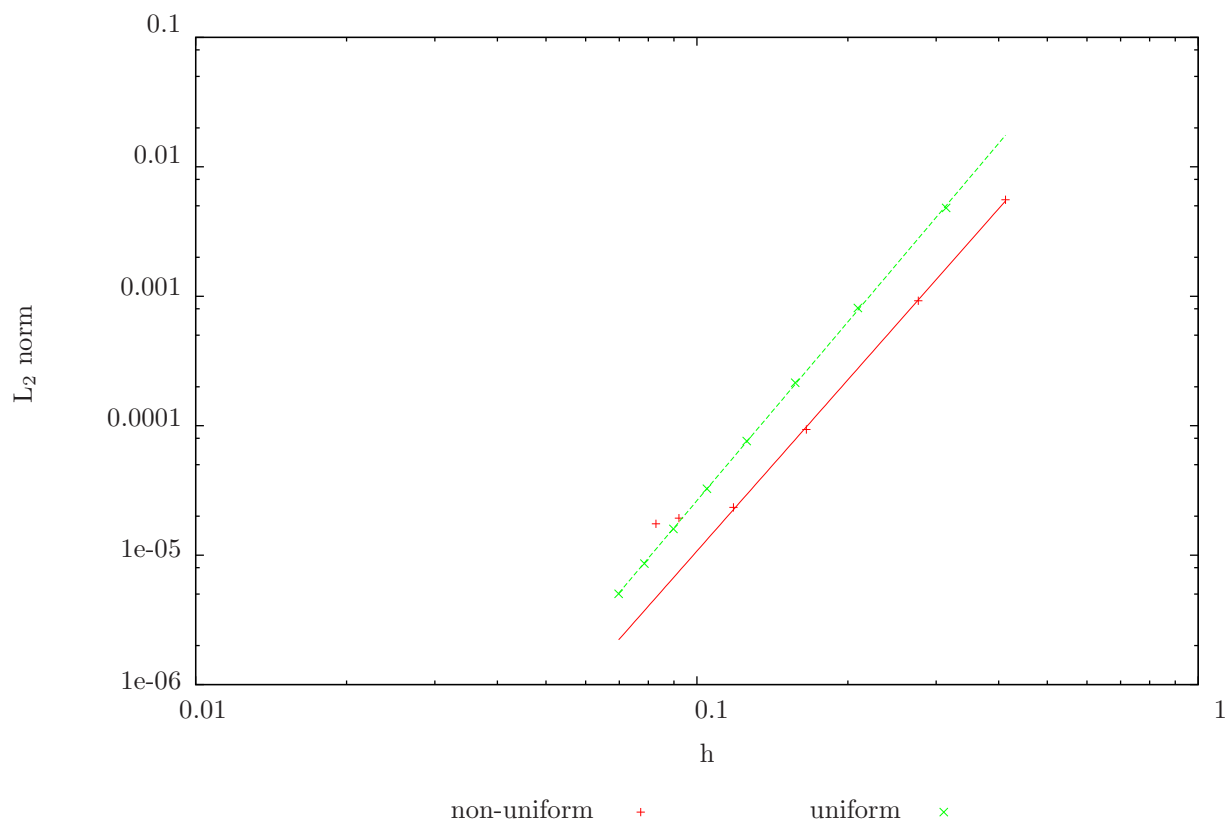
Fig. 6: Convergence test for the linear-acoustic equations.

American Institute of Aeronautics and Astronautics

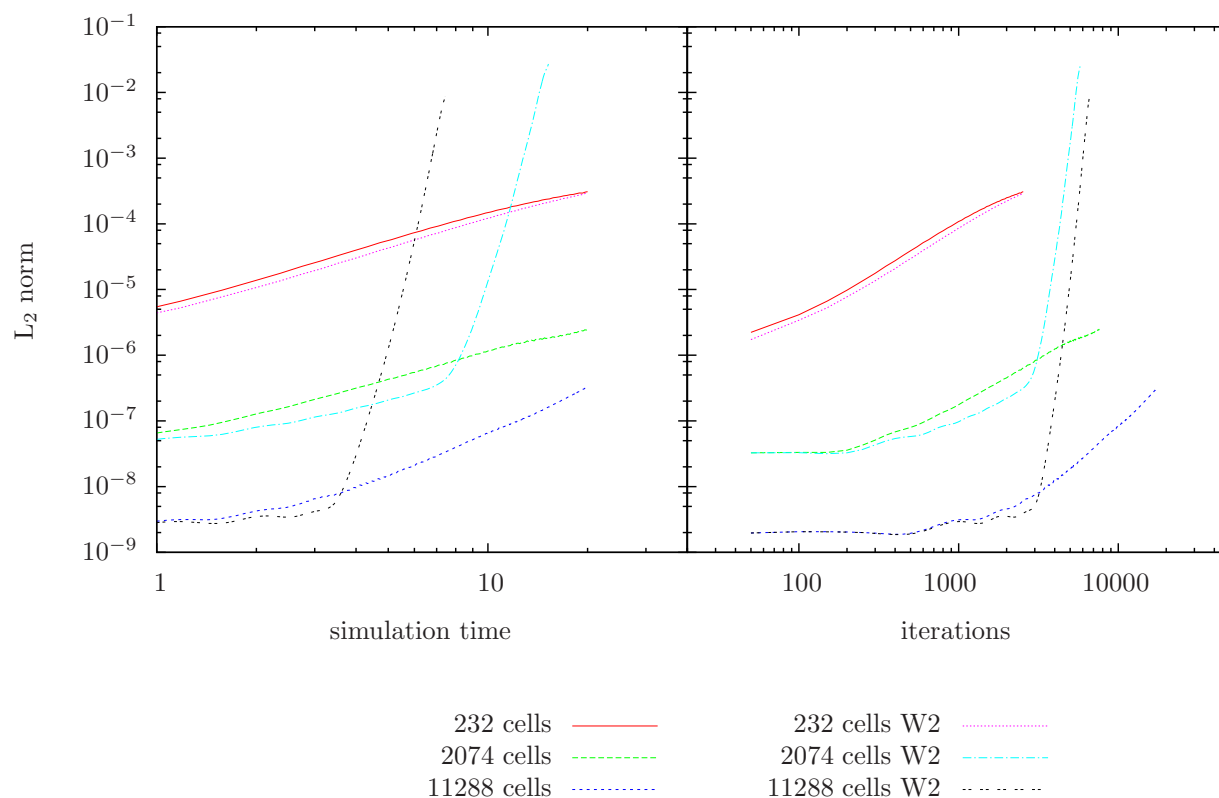Fig. 7: Convergence test for the Euler Equations
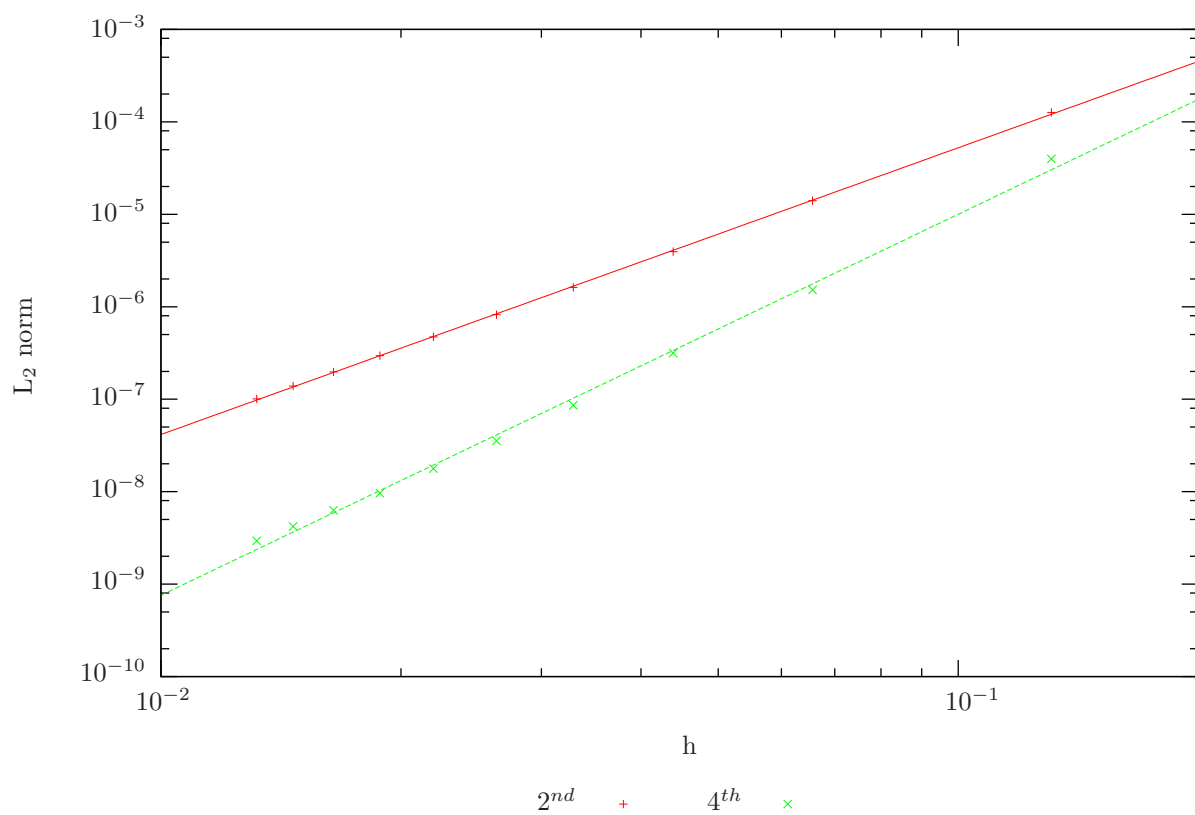
American Institute of Aeronautics and Astronautics

Fig. 8: Fourth order convergence test for the Euler Equations on an unstructured mesh.

References

[1]Chang, S., "A New Approach for Constructing Highly Stable High Order CESE Schemes," *48th AIAA Aerospace Science Meeting*, Vol. 2010-543, AIAA, Orlando, FL, Jan. 2010.

[2]Bilyeu, D., Chen, Y., and Yu, S. J., "High-Order CESE Methods for the Euler Equations," *49th AIAA Aerospace Sciences Meeting*, Vol. 2011-1065, AIAA, Orlando, Florida, Jan. 2011.

[3]Chang, S., "The Method of Space-Time Conservation Element and Solution Element – A New Approach for Solving the Navier-Stokes and Euler Equations," *Journal of Computational Physics*, Vol. 119, No. 2, July 1995, pp. 295–324.

[4]Wang, X. and Chang, S., "A 2D Non-Splitting Unstructured Triangular Mesh Euler Solver Based on the Space-Time Conservation Element and Solution Element Method," *Computational Fluid Dynamics JOURNAL*, Vol. 8, No. 2, 1999, pp. 309–325.

[5]Chang, S. and Wang, X., "Multi-Dimensional Courant Number Insensitive CE/SE Euler Solvers for Applications Involving Highly Nonuniform Meshes," *39th AIAA/ASME/SAE/ASEE Joint Propulsion Conference and Exhibit*, Huntsville, Alabama, July 2003.

[6]Wang, Z. J., "High-order methods for the Euler and Navier–Stokes equations on unstructured grids," *Progress in Aerospace Sciences*, Vol. 43, No. 1-3, 2007, pp. 1–41.
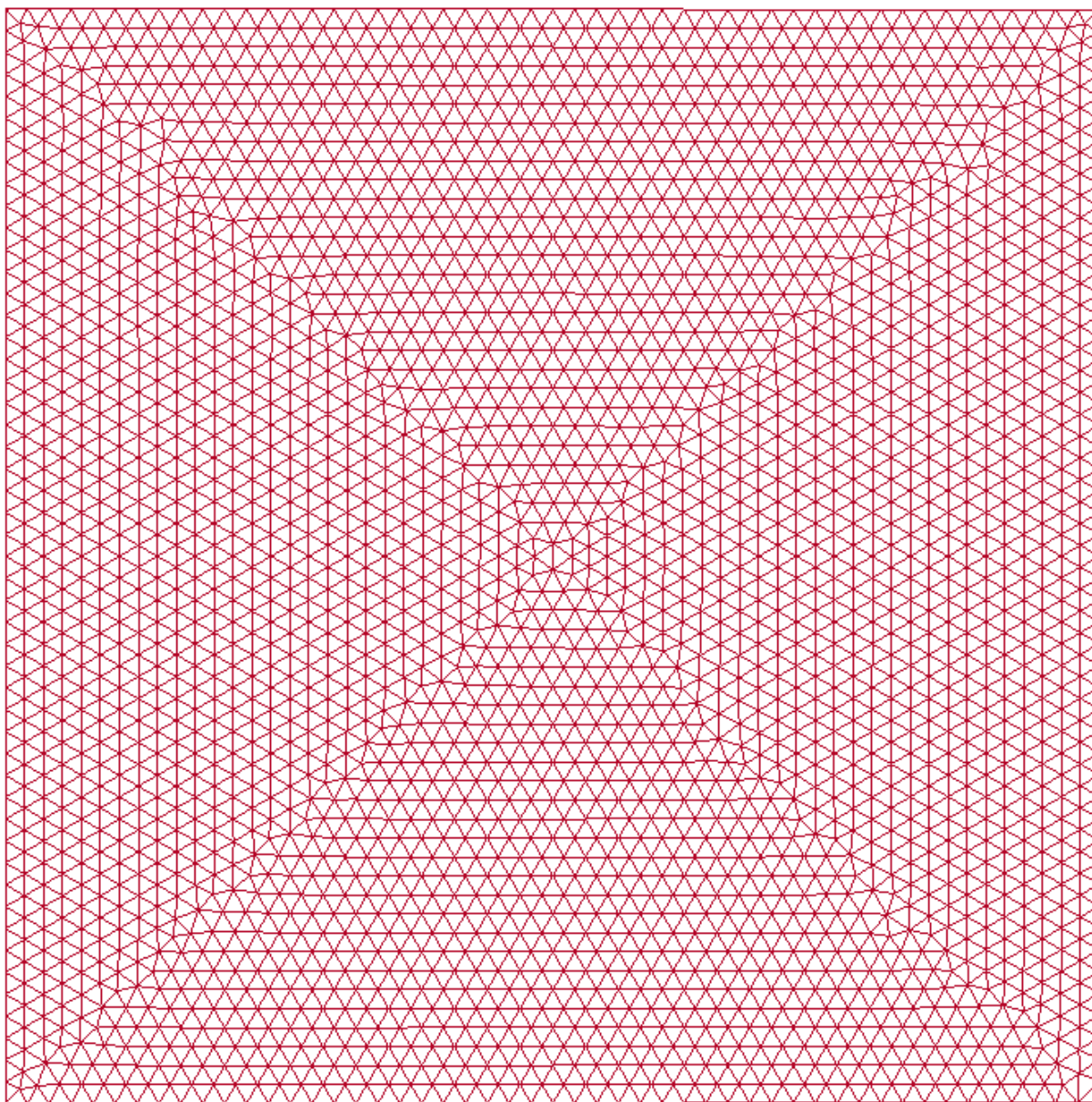
Fig. 9: An examle domain used in the shock case

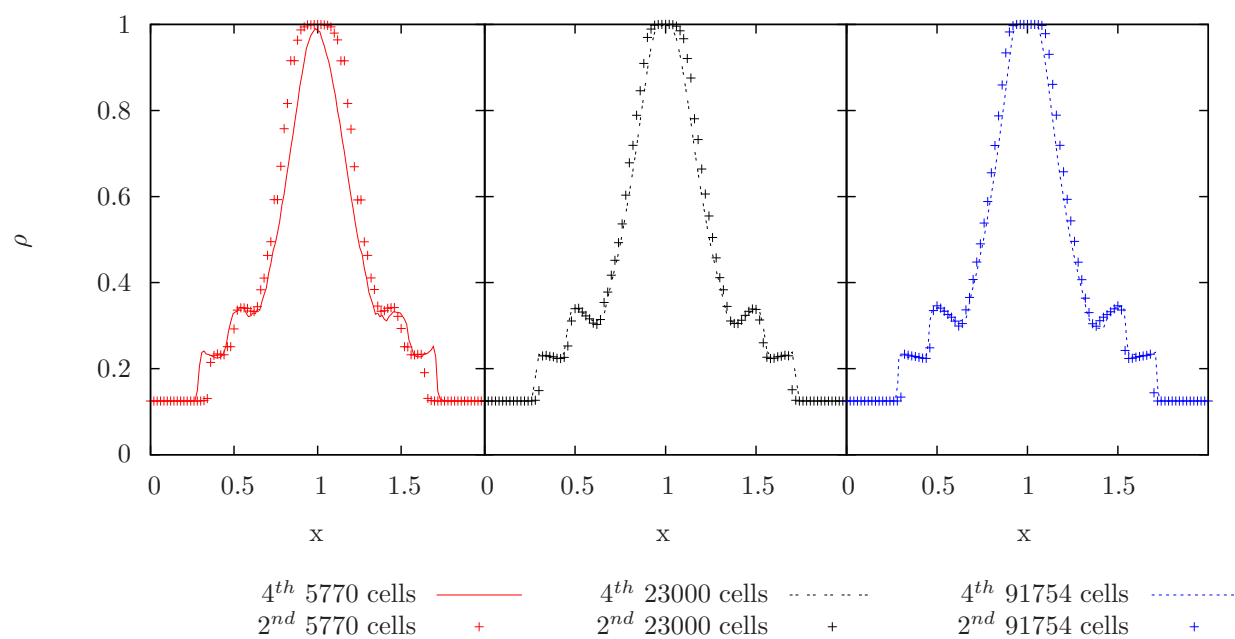American Institute of Aeronautics and Astronautics

Fig. 10: Comparison of the fourth- and second-order CESE schemes for capturing shocks at three different resolutions.

American Institute of Aeronautics and Astronautics